Electronic Supplementary Material (ESI) for Journal of Materials Chemistry A.
This journal is © The Royal Society of Chemistry 2018

Sprinkling $MnFe_2O_4$ quantum dots on nitrogen-doped graphene sheets: formation mechanism and application for high-performance supercapacitor electrodes

Lijun Su,[a,e] Shulai Lei,[a] Li Liu,[b] Lingyang Liu,[a,e] Yuefei Zhang,[c] Siqi Shi[d] and Xingbin Yan*[a]

[a.] *Laboratory of Clean Energy Chemistry and Materials, State Key Laboratory of Solid Lubrication, Lanzhou Institute of Chemical Physics, Chinese Academy of Sciences, Lanzhou 730000, P. R. China. *Email - xbyan@licp.cas.cn*

[b.] *State Key Laboratory for Oxo Synthesis and Selective Oxidation, Lanzhou Institute of Chemical Physics, Chinese Academy of Sciences, Lanzhou 730000, P. R. China.*

[c.] *Institute of Microstructure and Property of Advanced Materials, Beijing University of Technology, Beijing 100124, P. R. China*

[d.] *School of Materials Science and Engineering, Shanghai University, Shanghai 200444, P. R. China.*

[e.] *University of Chinese Academy of Sciences, Beijing 100080, P. R. China.*

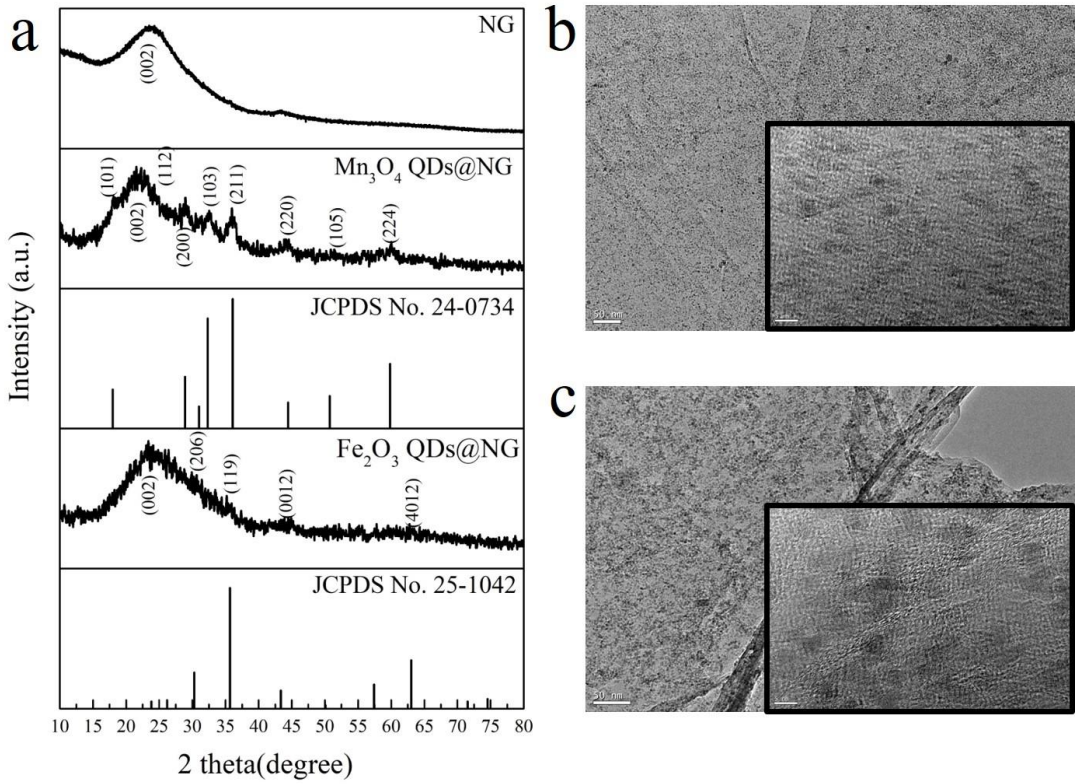

Figure S1. (a) XRD pattern of N-doped graphene (NG), Mn_3O_4 QDs@NG and Fe_2O_3 QDs@NG. TEM images of Fe_2O_3 QDs@NG (b) and Mn_3O_4 QDs@NG (c).

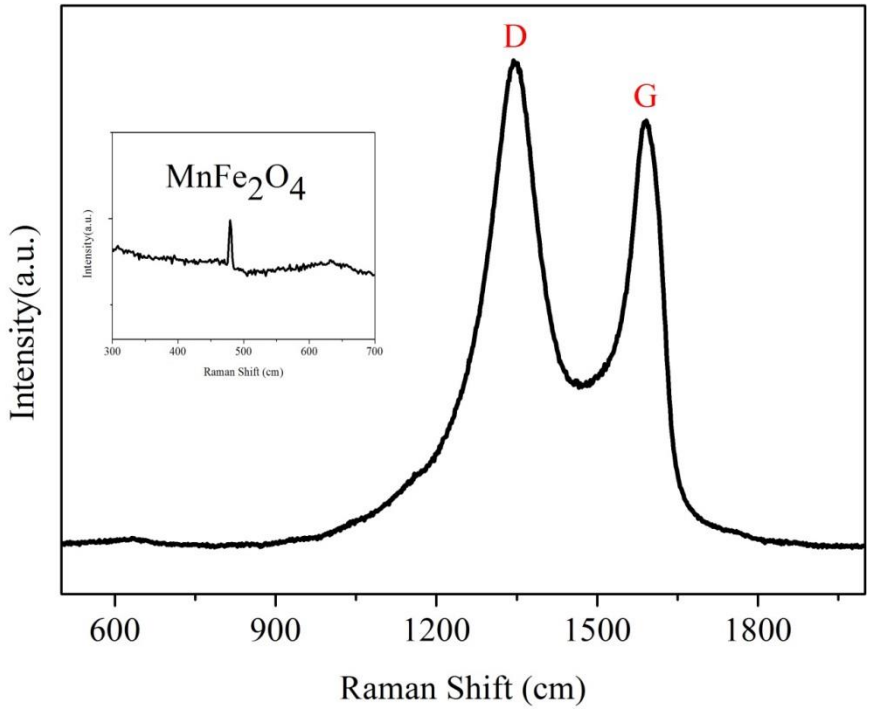

Figure S2. Raman spectrum of $MnFe_2O_4$ QDs@NG sample.

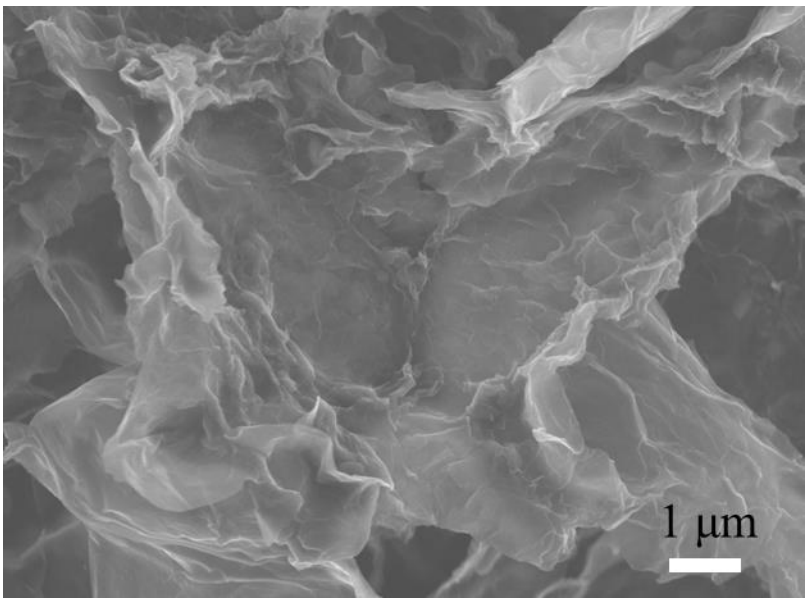

Figure S3. FESEM image of as-prepared $MnFe_2O_4$ QDs@NG (before annealing).

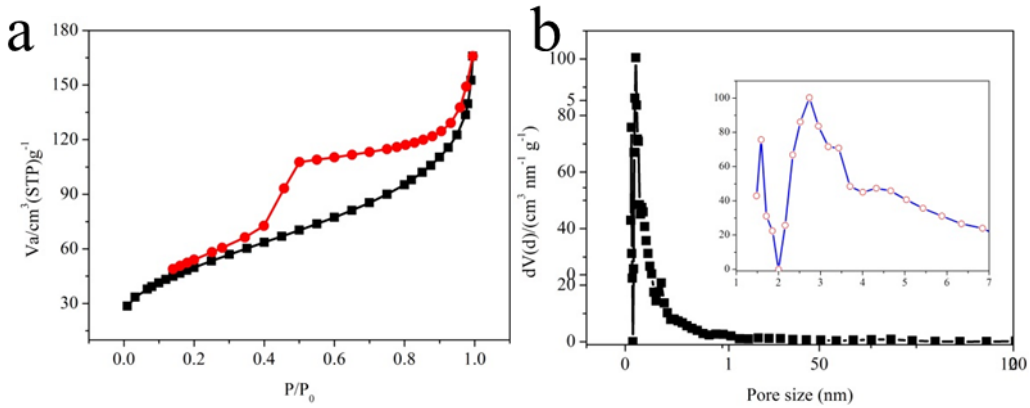

Figure S4. N_2 adsorption/desorption isotherms (a) and the corresponding pore-size distribution (b) of $MnFe_2O_4$ QDs@NG. (Inset is an enlarged curve of pore-size distribution.)

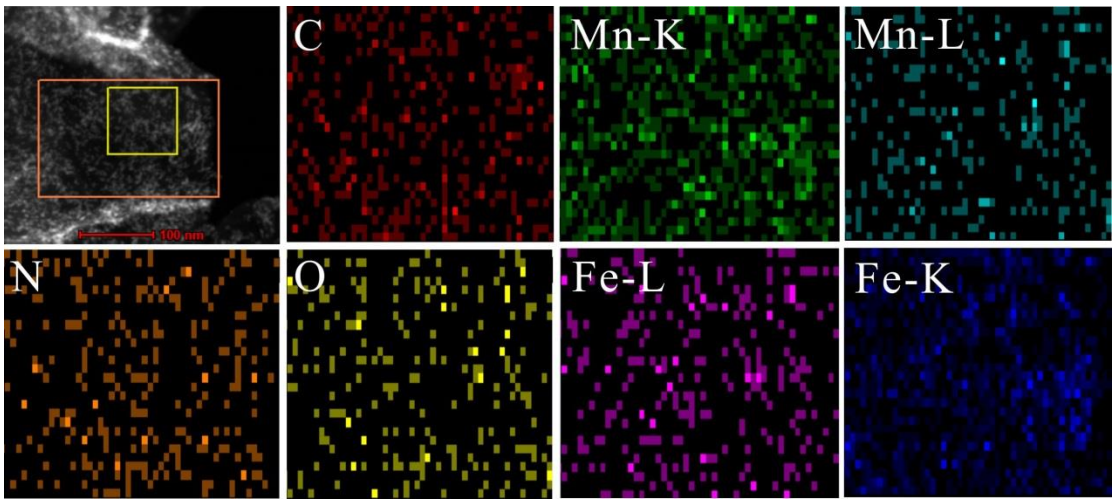

Figure S5. EDS mapping images of as-prepared $MnFe_2O_4$ QDs@NG sample.

Table S1. Different types of nitrogen as well as their corresponding contents in $MnFe_2O_4$ QDs@NG sample measured by XPS.

N types	Pyridinic	Pyrrolic	Graphitic
Content (wt%)	25.3%	51.8%	23.9%

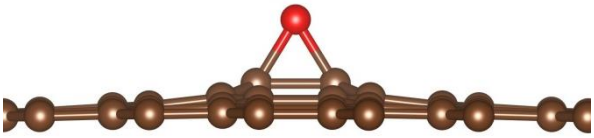

Figure S6. Side view of one epoxy group on graphene surface. Color code: carbon (brown), oxygen (red), all bond lengths are in Å.

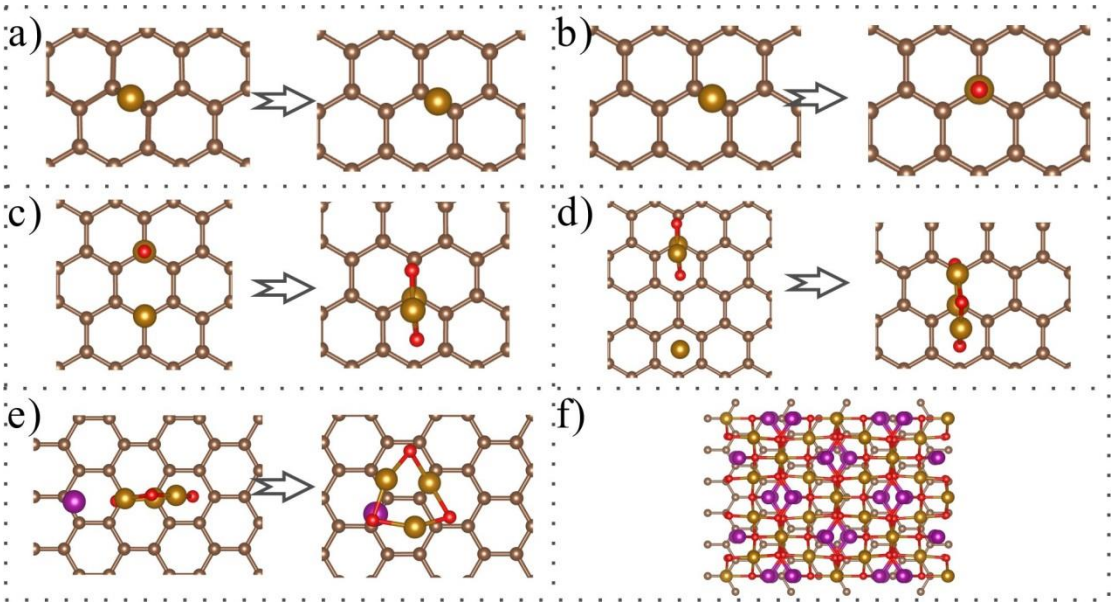

Figure S7. Top view of formation mechanism of $MnFe_2O_4$ QDs anchored on pristine GO surface. Each case was obtained by using DFT calculations. Color code: carbon (brown), oxygen (red), iron (yellow), manganese (purple), all bond lengths are in Å.

Table S2 The bond lengths calculated by DFT.

Bond length (Å)	a	b	c	d	e	f
①	1.62	1.64	1.75	1.81	1.94	3.79 *H(Mn)
②	2.95*H	2.17	1.75	1.79	1.90	3.55 *H (O)
③		2.17*H	1.87	1.80	1.90	3.70 *H (Fe)
④			1.85	1.79	1.79	
⑤			2.07	1.83	1.79	
⑥			2.06*H	1.83	1.85	
⑦				2.59*H	1.85	
					2.19*H(Mn)	
					2.46 *H(Fe)	

**H is the height of the lowest atom to the surface of GO.*

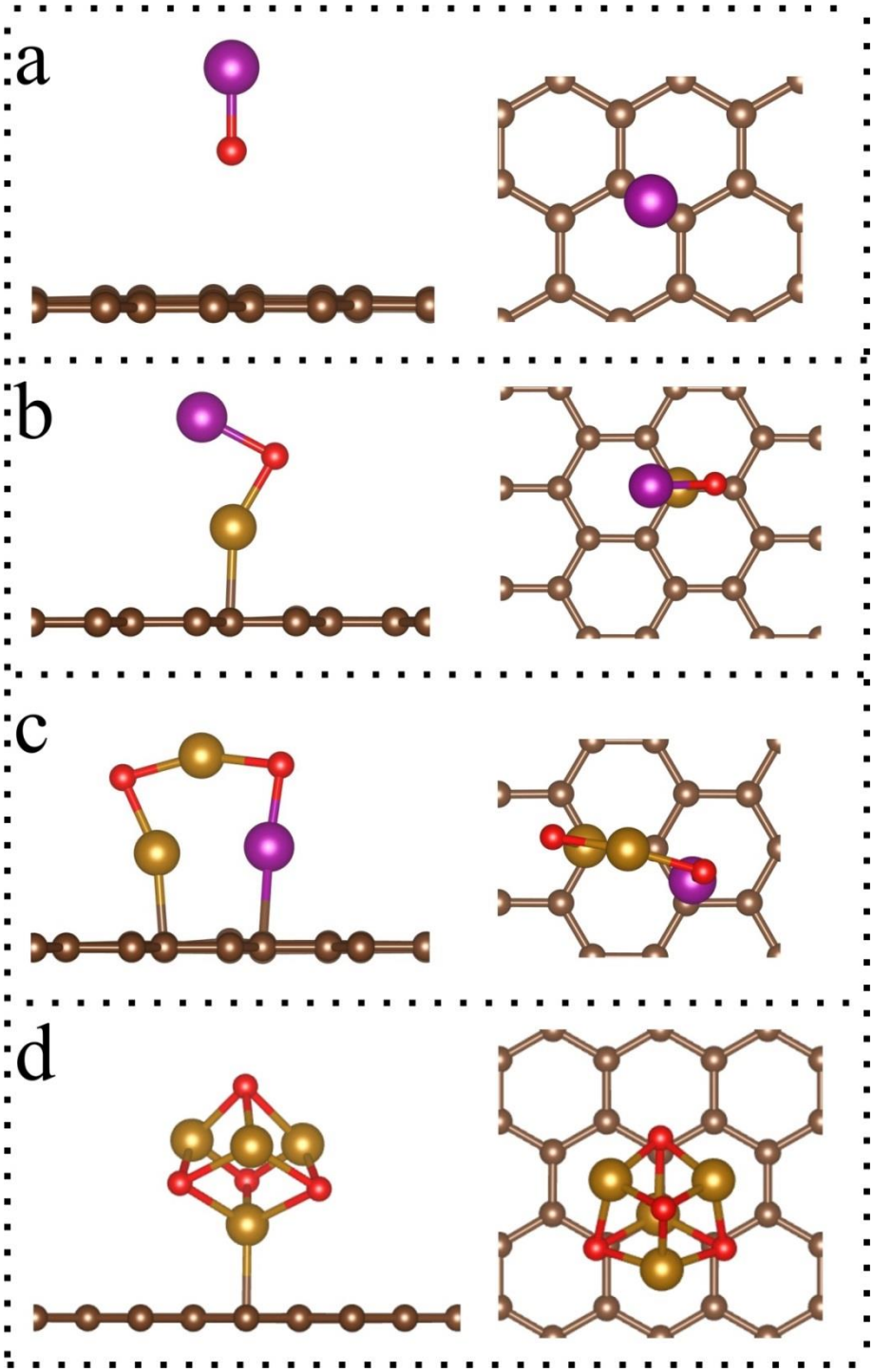

Figure S8. Side and top view of one Mn atom adsorb on graphene surface (a), one Mn atom adsorb on Fe-O group (b) and Mn atom adsorb on Fe_2O_2 group (c), one FeO_6 octahedra group formed on graphene surface (d). Color code: carbon (brown), oxygen (red), iron (yellow), manganese (purple), all bond lengths are in Å.

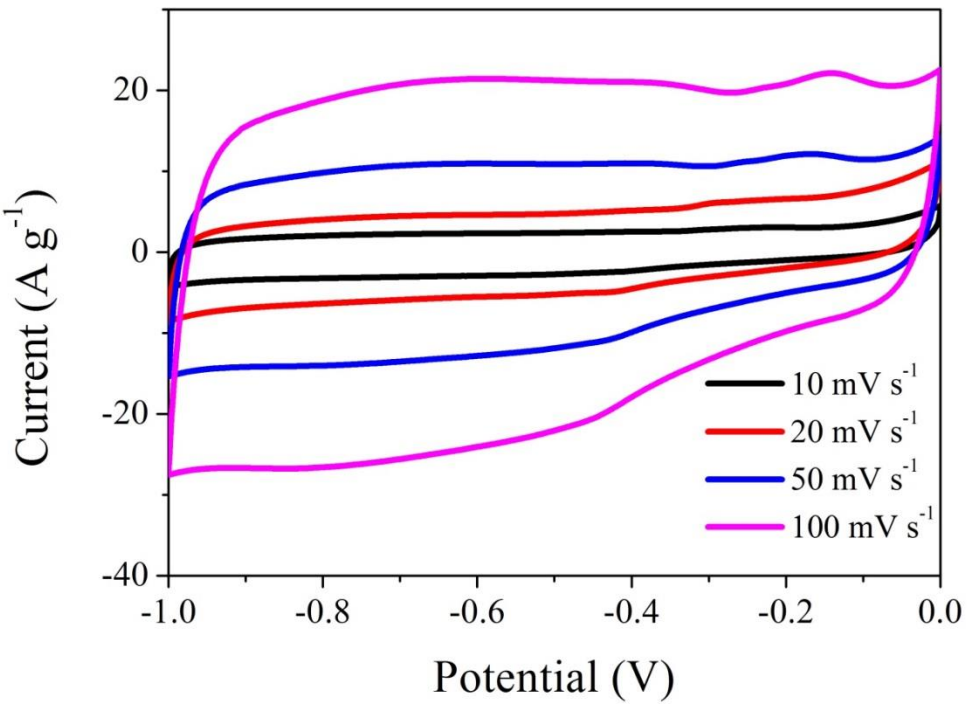

Figure S9. CV curves of pure NG at different scan rates.

The surface-reaction-controlled process and the diffusion-controlled process:

The total charge storage of $MnFe_2O_4$ QDs@NG electrode was semiquantitatively resolved by analyzing the current response of CV curves at different scan rates. In detail, the current (i) and the scan rate (v) keep to the following relationship:[1]

$$i = av^b \quad (1)$$

where both a and b are the adjustment constants. If the parameter b=0.5, the electrochemical reaction will be a diffusion-controlled process. If the parameter b=1, it will be a surface-reaction controlled process. As shown in Figure S10, the b was obtained from the plot of log(i) versus log(v) according to equation 1. Regarding to positive or negative scans, b values are all between 0.5 and 1, indicating that the total capacitive behavior of $MnFe_2O_4$ QDs@NG contains the surface-reaction-controlled

process and the diffusion-controlled process.[2] This complex process accords with the following relationship:

$$i(V) = k_1 + k_2 v^{1/2} \quad (2)$$

where k_1v is the surface-reaction-controlled current and $k_2v^{1/2}$ is the diffusion-controlled current. Then equation 2 can be changed to:

$$\frac{i(V)}{v^{1/2}} = k_1 v^{1/2} + k_2 \quad (3)$$

On the basis of the linear fitting of voltammetric currents at each potential, we can determine the coefficients k_1 and k_2, and calculate the k_1v and $k_2v^{1/2}$. Then the charge contributed from the capacitive current or diffusion-controlled current can be distinguished, as shown in Figure S11.[3-6]

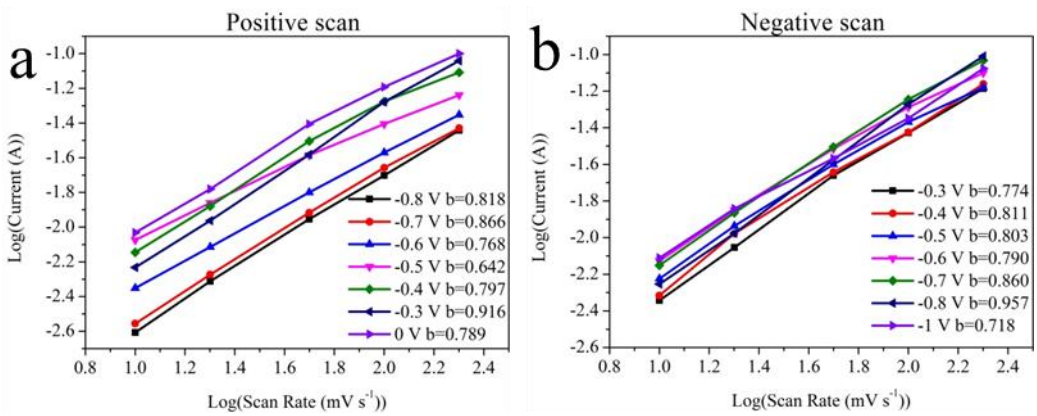

Figure S10. The dependence of cathodic (a) and anodic (b) current with sweep rate of $MnFe_2O_4$ QDs@NG.

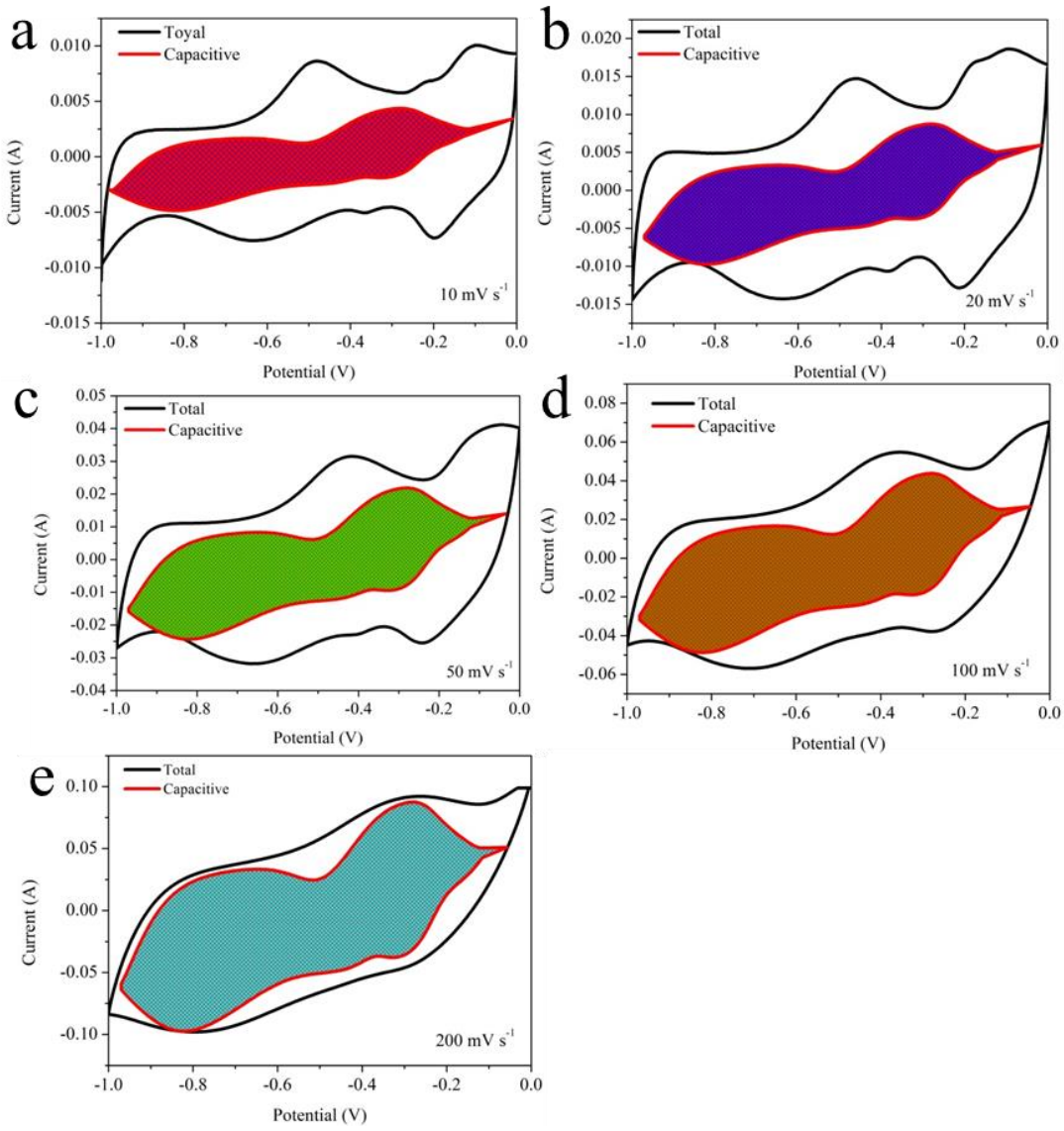

Figure S11. Cyclic voltammetry of $MnFe_2O_4$ QDs@NG tested in a 2 M KOH solution at (a) 10 mV s^{-1}, (b) 20 mV s^{-1}, (c) 50 mV s^{-1}, (d) 100 mV s^{-1} and (e) 200 mV s^{-1}. The shadowed areas represent the capacitive contribution.

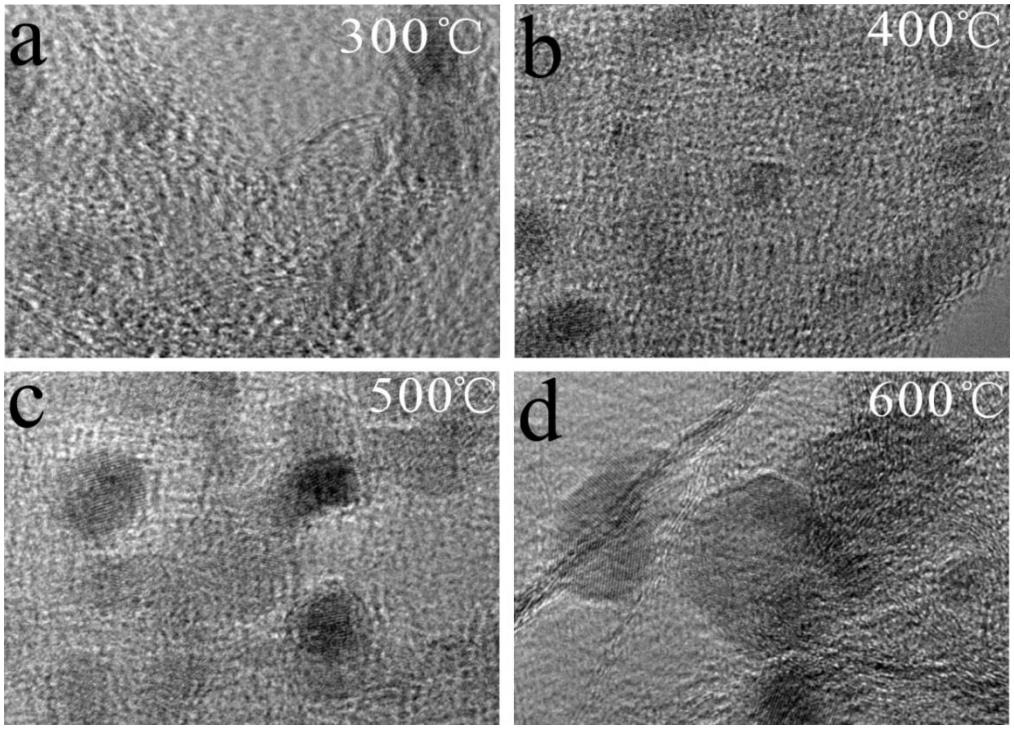

Figure S12. High resolution TEM images of $MnFe_2O_4$ QDs@NG after annealing at 300 (a),400 (b), 500 (c) and 600 ^oC (d), respectively.

Table S3. The average particle sizes of $MnFe_2O_4$ QDs prepared at different annealing conditions.

Temperature (^oC)	170	300	400	500	600
$MnFe_2O_4$ QDs@NG	3.3 nm	4.5 nm	4.8 nm	7 nm	14 nm
$MnFe_2O_4$ QDs@C-NG	3.3 nm	/	5 nm	5.2 nm	6.7 nm

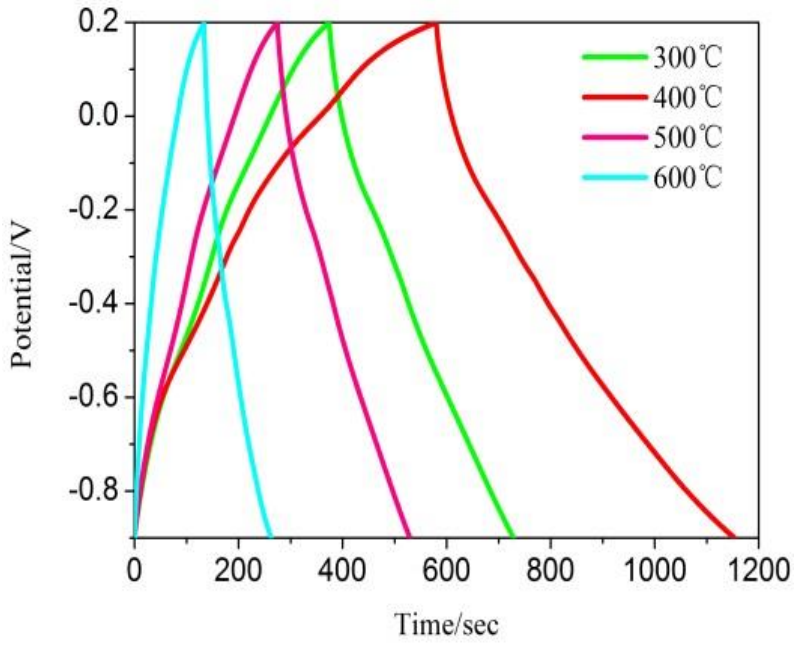

Figure S13. GCD curves of annealed $MnFe_2O_4$ QDs@NG samples at the same current density of 1 A g^{-1}.

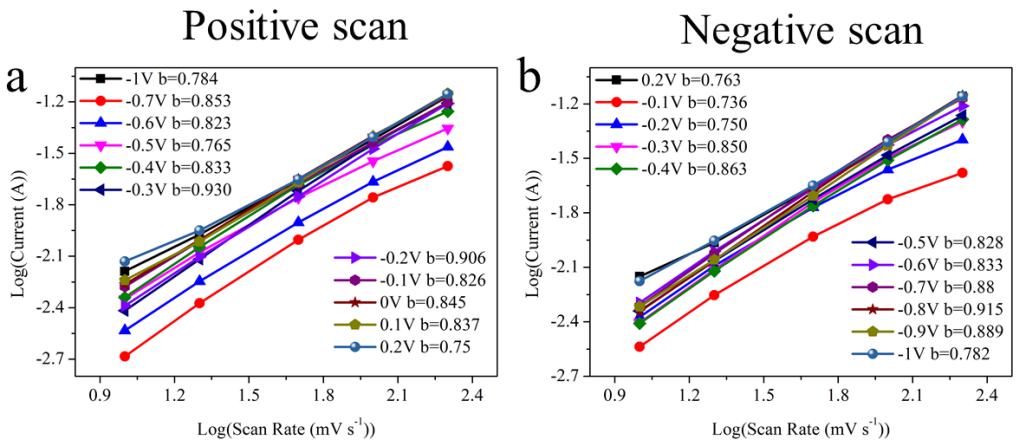

Figure S14. The dependence of cathodic (a) and anodic (b) current with sweep rate of $MnFe_2O_4$ QDs@NG-400.

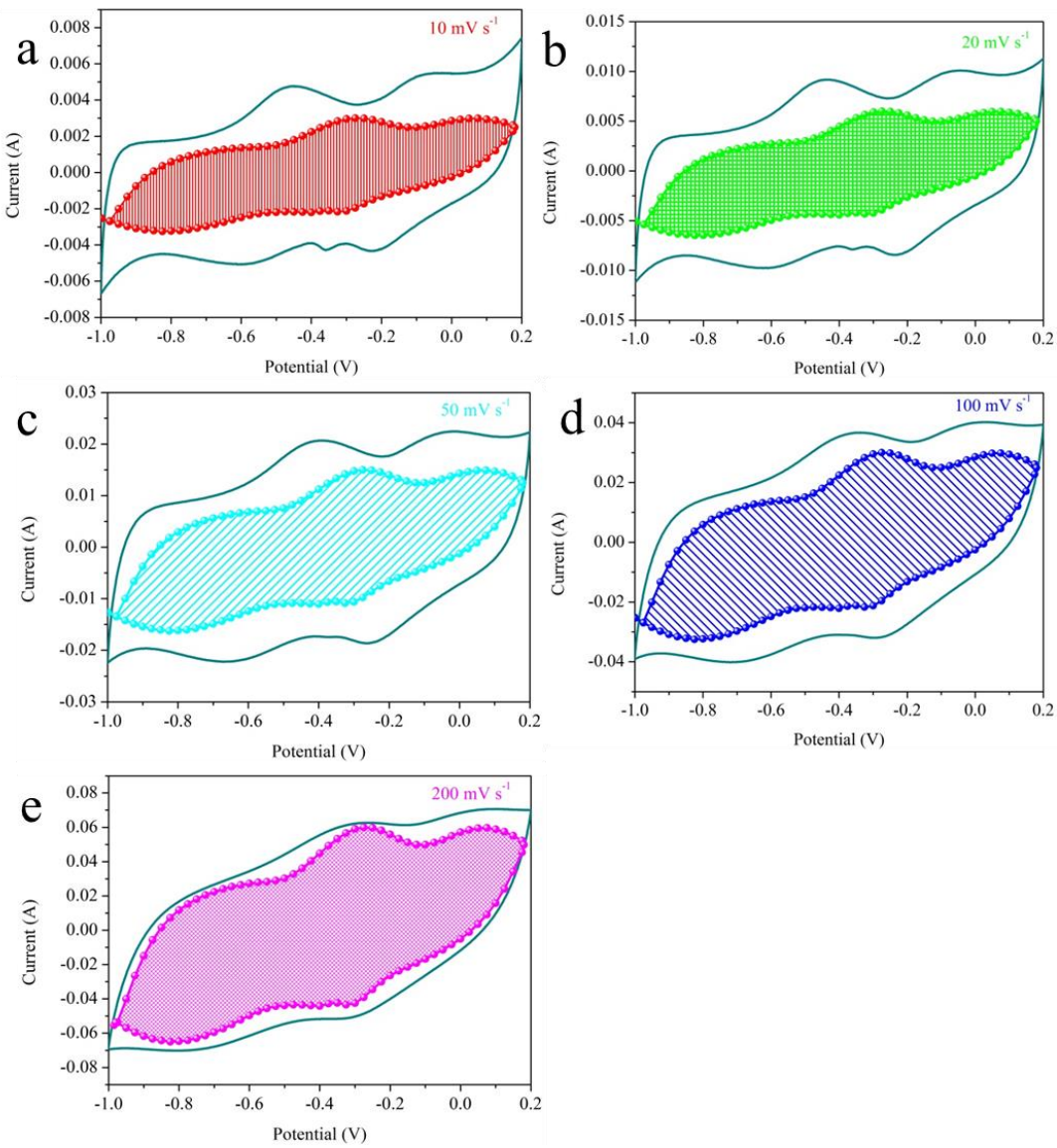

Figure S15. Cyclic voltammetry of $MnFe_2O_4$ QDs@NG-400 tested in a 2 M KOH solution at (a) 10 mV s^{-1}, (b) 20 mV s^{-1}, (c) 50 mV s^{-1}, (d) 100 mV s^{-1} and (e) 200 mV s^{-1}. The shadowed areas represent the capacitive contribution.

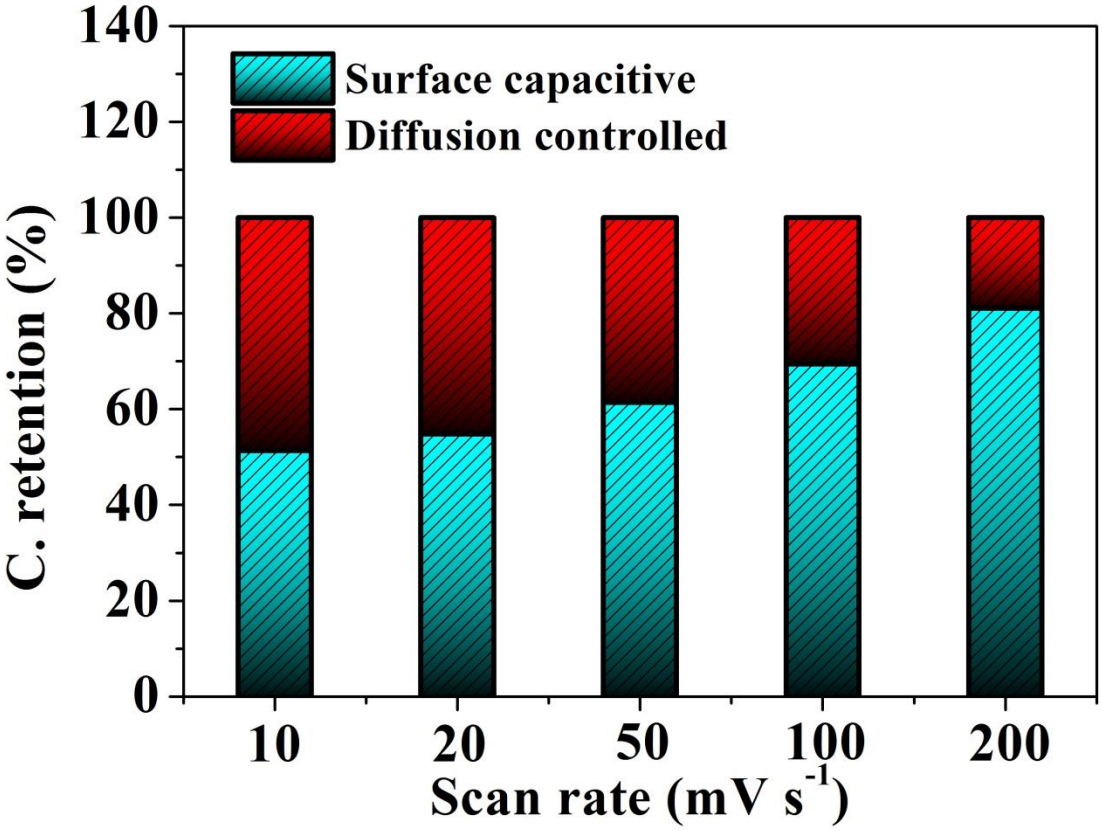

Figure S16. The capacitance contribution of $MnFe_2O_4$ QDs@NG-400 at different scan rates.

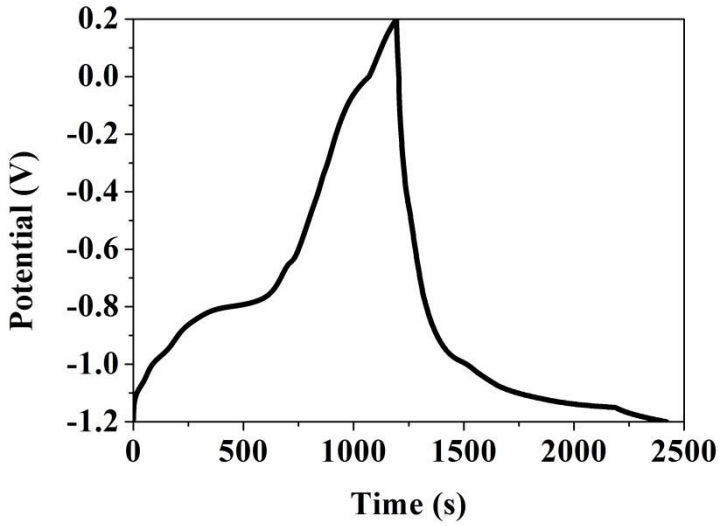

Figure S17. GCD curve of $MnFe_2O_4$ QDs@NG-400 electrode between -1.2 to 0.2 V at the current density of 1 A g^{-1}.

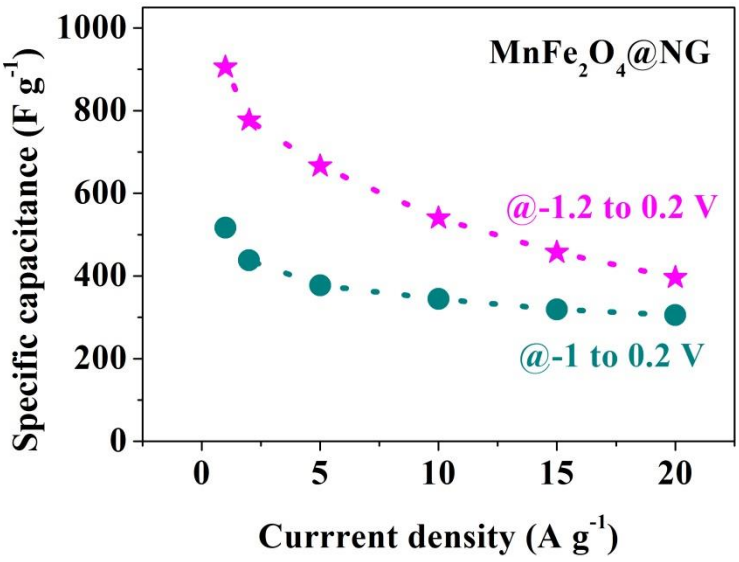

Figure S18. The specific capacitance of $MnFe_2O_4$ QDs@NG-400 electrode in different voltage windows of -1 to 0.2 V and -1.2 to 0.2 V at different scan rates.

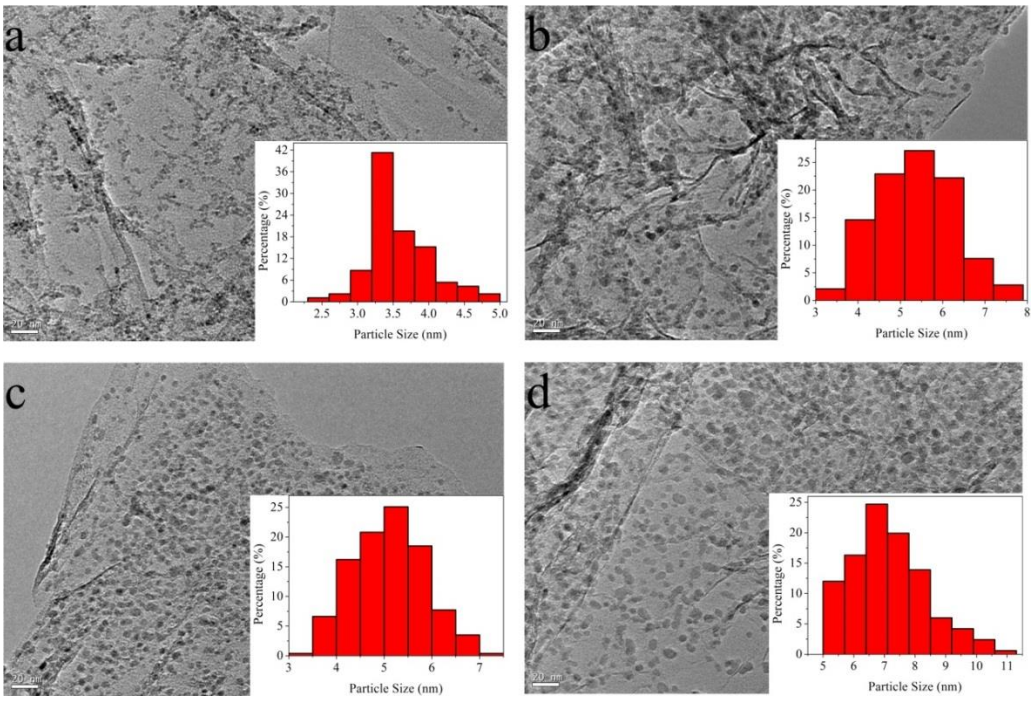

Figure S19. TEM images of $MnFe_2O_4$ QDs@C-NG samples: (a) before annealing and annealing at 400 (b), 500 (c) and 600 ^{o}C (d), respectively. Inserts are the corresponding size distributions of $MnFe_2O_4$ QDs.

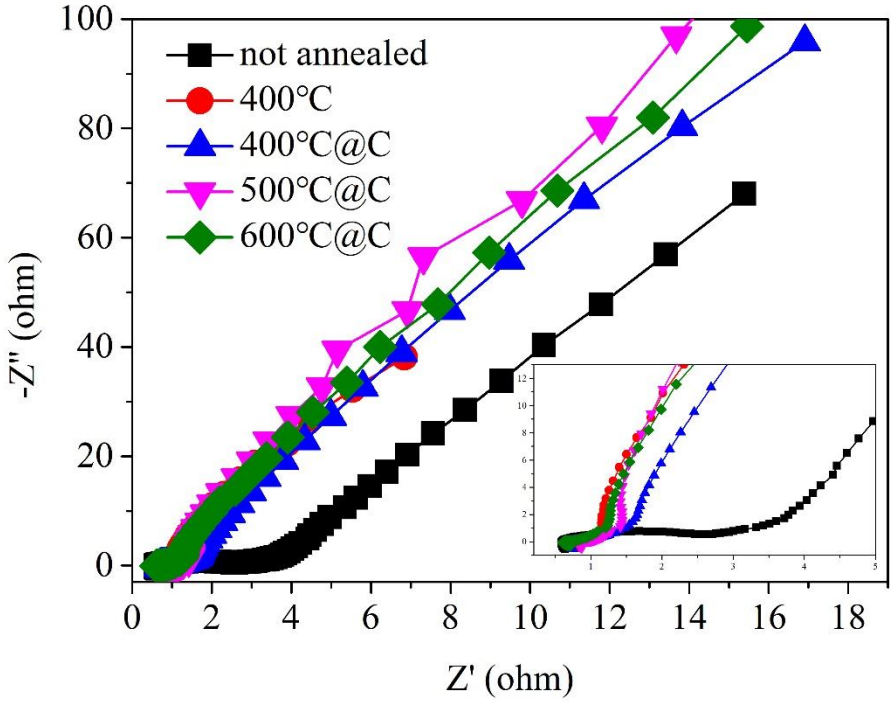

Figure S20. The electrochemical impedance spectroscopy (EIS) of different materials in Fig. 7h.

Table S4. Comparison of the overall performances between the recently reported negative materials of supercapacitors with our material in this work.

Anode materials	Electrolyte potential range (V)	Specific capacitance (F g^{-1})	Rate capability (F g^{-1})	Cycling stability	Refs (year)
Fe_2O_3 QDs @ FGS	1 M Na_2SO_4 -1 to 0 V	347 at 10 mV s^{-1}	140 at 1600 mV s^{-1}	95% after 5000 cycles at 0.5 A g^{-1}	(2014) Adv. Funct. Mater.[7]
FeOOH QDs @ FGS	1 M Li_2SO_4 -0.8 to 0 V	365 at 10 mV s^{-1}	189 at 128 A g^{-1}	89.7% after 20000 cycles at 4 A g^{-1}	(2015) Adv. Funct. Mater.[8]

	1 M Li_2SO_4 -1 to 0 V	403 at 5 mV s^{-1}			(2015) Adv. Funct. Mater.[8]
	1 M Li_2SO_4 -1.25 to 0 V	1243 at 5 mV s^{-1}			(2015) Adv. Funct. Mater.[8]
RuO_2 @ GSCs	1 M H_2SO_4 -0.2 to 0.8 V	570 at 1 mV s^{-1}	268 at 50 mV s^{-1}	97.9% after 1000 cycles at 1 A g^{-1}	(2010) Adv. Funct. Mater.[9]
GF-CNT@Fe_2O_3	2 M KOH -1.2 to 0 V	470.5 at 20 mA cm^{-1}	About 350 at 40 mA cm^{-1}	95.4% after 50000 cycles at 20 mA cm^{-1}	(2015) ACS Nano[10]
α-Fe_2O_3/graphene	1 M Na_2SO_4 -1.2 to -0.2 V	306 at 3 A g^{-1}	98.2 at 10 A g^{-1}	91.5% after 2000 cycles at 5 A g^{-1}	(2014) Small[11]
N-rGO/α-Fe_2O_3	1 M KOH -1.0 to 0 V	268.4 at 2 A g^{-1}	137 at 5 A g^{-1}	95.8% after 2000 cycles at 3 A g^{-1}	(2015) J. Solid State Electr.[12]
nitrogen-doped graphene/Fe_2O_3	1 M Na_2SO_4 -1.1 to -0.1 V	260.1 at 2 A g^{-1}	110.4 at 7 A g^{-1}	82.5% after 1000 cycles at 2 A g^{-1}	(2014) J. Alloy. Compd.[13]
rGO/$MnFe_2O_4$	6 M KOH -1 to 0 V	276.9 at 10 mV s^{-1}	220 at 20 A g^{-1}	71% after 1000 cycles at 10 A g^{-1}	(2014) JPN J. Appl. Phys.[14]
$MnFe_2O_4$/graphene/ PANI	1 M NaCl -0.6 to 0.3 V	338 at 0.5 mA cm^{-2}	150 at 5 mA cm^{-2}	100 % after 2000 cycles at 15 mA cm^{-2}	(2014) RSC Adv.[15]
$MnFe_2O_4$/graphene	1 M NaCl -0.55 to	241 at 0.5		100 % after 5000	(2015) J. Power Sources[16]

/PANI	0.25 V	mA cm^{-2}		cycles at 5 mA cm^{-2}	
$MnFe_2O_4$ QDs@NG	**2 M KOH -1.2 to 0.2 V**	**905 at 1 A g^{-1}**			**This work**
$MnFe_2O_4$ QDs@NG	**2 M KOH -1 to 0.2 V**	**517 at 1 A g^{-1}**		**60% after 23000 cycles at 2 A g^{-1}**	**This work**
$MnFe_2O_4$ QDs@C-NG	**2 M KOH -1.1 to 0.2 V**	**450 at 1 A g^{-1}**	**150 F g^{-1} at 200 A g^{-1}**	**83% after 65000 cycles at 2 A g^{-1}**	**This work**

References

1. T. Brezesinski, J. Wang, J. Polleux, B. Dunn and S. H. Tolbert, *J. Am. Chem. Soc.*, 2009, **131**, 1802.
2. J. Wang, J. Polleux, A. James Lim and B. Dunn, *J. Phys. Chem. C*, 2007, **111**, 14925-14931.
3. T. C. Liu, *J. Electrochem. Soc.*, 1998, **145**, 1882-1888.
4. B. Laskova, M. Zukalova, A. Zukal, M. Bousa and L. Kavan, *J. Power Sources*, 2014, **246**, 103-109.
5. R. Li and J. Liu, *Electrochim. Acta*, 2014, **120**, 52-56.
6. Z. Chen, D. Weng, X. Wang, Y. Cheng, G. Wang and Y. Lu, *Chem. Commun.*, 2012, **48**, 3736.
7. H. Xia, C. Hong, B. Li, B. Zhao, Z. Lin, M. Zheng, S. V. Savilov and S. M. Aldoshin, *Adv. Funct. Mater.*, 2015, **25**, 627-635.
8. J. Liu, M. Zheng, X. Shi, H. Zeng and H. Xia, *Adv. Funct. Mater.*, 2016, **26**, 919-930.
9. Z. S. Wu, D. W. Wang, W. Ren, J. Zhao, G. Zhou, F. Li and H. M. Cheng, *Adv. Funct. Mater.*, 2010, **20**, 3595-3602.
10. C. Guan, J. Liu, Y. Wang, L. Mao, Z. Fan, Z. Shen, H. Zhang and J. Wang, *ACS Nano*, 2015, **9**, 5198-5207.
11. Y. S, S. X, Z. P, S. J and G. L, *Small*, 2014, **10**, 2270.
12. H. D. Liu, J. L. Zhang, D. D. Xu, L. H. Huang, S. Z. Tan and W. J. Mai, *J. Solid State Electr.*, 2015, **19**, 135-144.
13. P. Zhao, W. Li, G. Wang, B. Yu, X. Li, J. Bai and Z. Ren, *J. Alloy. Compd.*, 2014, **604**, 87-93.
14. I. Kotutha, E. Swatsitang, W. Meewassana and S. Maensiri, *JPN J. Appl. Phys.*, 2015, **54**, 06FH10.
15. K. V. Sankar and R. K. Selvan, *RSC Adv.*, 2014, **4**, 17555.
16. K. V. Sankar and R. K. Selvan, *J. Power Sources*, 2015, **275**, 399-407.